

# Regularity and finite element approximation for two-dimensional elliptic equations with line Dirac sources

Hengguang Li<sup>a</sup>, Xiang Wan<sup>b</sup>, Peimeng Yin<sup>a,\*</sup>, Lewei Zhao<sup>c</sup>

<sup>a</sup> Wayne State University, Department of Mathematics, Detroit, MI 48202, United States of America

<sup>b</sup> The George Washington University, Department of Mathematics, Washington, DC 20052, United States of America

<sup>c</sup> Beaumont Health System, Department of Radiation Oncology, Royal Oak, MI 48073, United States of America

## ARTICLE INFO

### Article history:

Received 16 May 2020

Received in revised form 17 February 2021

### Keywords:

Singular line

Weighted Sobolev space

Regularity

Finite element method

Graded meshes

## ABSTRACT

We study the elliptic equation with a line Dirac delta function as the source term subject to the Dirichlet boundary condition in a two-dimensional domain. Such a line Dirac measure causes different types of solution singularities in the neighborhood of the line fracture. We establish new regularity results for the solution in a class of weighted Sobolev spaces and propose finite element algorithms that approximate the singular solution at the optimal convergence rate. Numerical tests are presented to justify the theoretical findings.

© 2021 Elsevier B.V. All rights reserved.

## 1. Introduction

Let  $\Omega \subset \mathbb{R}^2$  be a polygonal domain and let  $\gamma$  be a line segment strictly contained in  $\Omega$ . Consider the elliptic boundary value problem

$$\begin{cases} -\Delta u = \delta_\gamma & \text{in } \Omega, \\ u = 0 & \text{on } \partial\Omega, \end{cases} \quad (1.1)$$

where the source term  $\delta_\gamma$  is the line Dirac measure on  $\gamma$ , namely,

$$\langle \delta_\gamma, v \rangle = \int_\gamma v(s) ds, \quad \forall v \in L^2(\gamma).$$

Such equations occur in many mathematical models including monophasic flows in porous media, tissue perfusion or drug delivery by a network of blood vessels [1] and elliptic optimal control problems with controls acting on a lower dimensional manifold [2]. Note that the line Dirac measure  $\delta_\gamma$  is not an  $L^2$  function. Although the solution tends to be smooth in a large part of the domain, it can become singular in the region close to the one-dimensional (1D) fracture  $\gamma$  and in the region close to the vertices of the domain, where the corner singularities are expected to rise. Since the corner singularity associated to Eq. (1.1) is understood fairly well in the literature, we shall address the concerns on the regularity of the solution near  $\gamma$  and on the efficacy of the numerical approximation.

Finite element approximations for second order elliptic equations with singular source terms have attracted considerable attention and many studies have focused on point singular measures. Babuška [3], Scott [4,5], and Casas [6] studied the convergence in the  $L^2$  (or  $H^\epsilon$  with small  $\epsilon$ ) norm for Dirac measures centered at some points in 2D; and a review of

\* Corresponding author.

E-mail addresses: [li@wayne.edu](mailto:li@wayne.edu) (H. Li), [xiangwan@gwu.edu](mailto:xiangwan@gwu.edu) (X. Wan), [pyin@wayne.edu](mailto:pyin@wayne.edu) (P. Yin), [Lewei.Zhao@beaumont.org](mailto:Lewei.Zhao@beaumont.org) (L. Zhao).

the convergence rates can be found in [7], in which the authors considered the Dirac measures centered at some points in both 2D and 3D and showed that for  $P_1$  finite elements quasi-optimal order and for higher order finite elements optimal order a priori estimates on a family of quasi-uniform meshes in  $L^2$ -norm on a subdomain excludes the locations of the delta source terms. For a Dirac measure centered at a point in a  $N$ -dimensional domain with  $N \geq 2$ , locally refined meshes around the singular point were used in [8] to improve the convergence rate. Graded meshes were used in [9] to study the convergence rate of the finite element approximation for a point Dirac measure in 2D and  $L^2$  error estimate of order  $h^2 |\ln h|^{\frac{3}{2}}$  was obtained for approximations based on  $P_1$  polynomials. More recently, 1D singular source terms have also attracted some attention. In [10,11], finite element immersed interface methods were studied for interfaces problems, which can be written as (1.1) with  $\gamma$  being a closed loop. By assuming the regularity of an elliptic equation in 3D with a Dirac measure concentrated on a 1D fracture in a weighted Sobolev space, optimal finite element convergence rates were obtained in [1,12] by using graded meshes. Then the authors in [13] derived the 3D regularity for the simplified equation in [1,12] when the Dirac measure concentrated on a line or segment fracture.

In this paper, we derive regularity estimates and propose optimal finite element algorithms for Eq. (1.1). In particular, we investigate the solution regularity in a class of Kondratiev-type weighted spaces. Note that the smoothness of the solution varies in different parts of the domain: the region close to the vertices, the neighborhood of the fracture  $\gamma$ , and the rest of the domain (Remark 3.1). By studying the local problem that inherits the line Dirac measure from Eq. (1.1), we obtain a “full-regularity” estimate in these weighted spaces in the neighborhood of  $\gamma$ . The key idea is to exploit the connection between the line Dirac measure and proper elliptic transmission problems in these weighted spaces. Based on the new regularity results and the existing regularity estimates on corner singularities, we in turn propose graded mesh refinement algorithms, such that the associated finite element methods of any order recover the optimal convergence rate in the energy norm even when the solution is singular. We study the model problem (1.1) with a simple line fracture to simplify the exposition and avoid nonessential complications in analysis. These results can be extended to more general cases, including the case where the single line fracture is replaced by multiple line fractures, whether intersecting or non-intersecting. With proper modifications, we also expect these analytical tools will be useful in the case when  $\gamma$  is a smooth curve and when the source term  $\delta_\gamma$  is replaced by  $q\delta_\gamma$  for  $q \in L^2(\gamma)$ .

The rest of the paper is organized as follows. In Section 2, we discuss the well-posedness and global regularity of Eq. (1.1) in Sobolev spaces. In Section 3, we introduce the weighted spaces and derive the regularity estimates for the solution in the neighborhood of  $\gamma$ . The main regularity results, summarized in Theorem 3.8, imply that in addition to the lack of regularity in the direction across  $\gamma$ , the solution also possesses isotropic singularities at the endpoints of the line fracture. In Section 4, we propose the finite element approximation of Eq. (1.1) based on a simple and explicit construction of graded meshes (Algorithm 4.1 and Remark 4.2). We further show that the proposed numerical methods achieve the optimal convergence rate by local interpolation error analysis in weighted spaces. We present various numerical test results in Section 5 to validate the theory.

Throughout the text below, we denote by  $ab$  the line segment with endpoints  $a$  and  $b$ . The generic constant  $C > 0$  in our estimates may be different at different occurrences. It will depend on the computational domain, but not on the functions involved or the mesh level in the finite element algorithms.

## 2. Well-posedness and regularity in Sobolev spaces

### 2.1. Well-posedness of the solution

Denote by  $H^m(\Omega)$ ,  $m \geq 0$ , the Sobolev space that consists of functions whose  $i$ th ( $0 \leq i \leq m$ ) derivatives are square integrable. Let  $L^2(\Omega) := H^0(\Omega)$ . Denote by  $H_0^1(\Omega) \subset H^1(\Omega)$  the subspace consisting of functions with zero trace on the boundary  $\partial\Omega$ . The variational formulation for Eq. (1.1) is

$$a(u, v) := \int_{\Omega} \nabla u \cdot \nabla v dx = \langle \delta_\gamma, v \rangle, \quad \forall v \in H_0^1(\Omega). \tag{2.1}$$

According to the trace estimate [14],  $v|_\gamma$  is well defined in  $L^2(\gamma)$  for  $v \in H^1(\Omega)$ . Therefore, it is clear that there exists a unique solution  $u \in H_0^1(\Omega)$  defined by (2.1). However, the solution has limited regularity because of the singular source term  $\delta_\gamma \notin L^2(\Omega)$ . In the rest of this section, we present the global regularity estimates for the solution in the domain.

### 2.2. Regularity in Sobolev spaces

We begin with the regularity estimates of problem (1.1) in Sobolev spaces  $H^m$ . We first have the following result regarding the line Dirac measure  $\delta_\gamma$ .

**Lemma 2.1.** *Let  $\Omega \subset \mathbb{R}^2$  be a bounded domain. Then  $\delta_\gamma \in H^{-\frac{1}{2}-\epsilon}(\Omega)$  for any  $\epsilon > 0$ .*

**Proof.** The proof is based on the duality pairing (cf. [14]). Given  $\epsilon > 0$  and  $v \in H^{\frac{1}{2}+\epsilon}(\Omega)$ , by Hölder’s inequality and the trace estimate [14,15], we have

$$\langle \delta_\gamma, v \rangle = \int_\gamma v(s) ds \leq C \|v\|_{L^2(\gamma)} \leq C \|v\|_{H^{\frac{1}{2}+\epsilon}(\Omega)}.$$

Therefore, by the standard definition, we have

$$\|\delta_\gamma\|_{H^{-\frac{1}{2}-\epsilon}(\Omega)} := \sup\{\langle \delta_\gamma, v \rangle : \|v\|_{H^{\frac{1}{2}+\epsilon}(\Omega)} = 1\} \leq C,$$

which completes the proof.  $\square$

Consequently, we have the following global regularity estimate for the solution.

**Lemma 2.2.** *Given  $\epsilon > 0$ , the solution of Eq. (1.1) satisfies  $u \in H^{\frac{3}{2}-\epsilon}(\Omega) \cap H_0^1(\Omega)$ .*

**Proof.** From Lemma 2.1, it follows  $\delta_\gamma \in H^{-\frac{1}{2}-\epsilon}(\Omega)$ . Then the standard elliptic regularity theory [16] leads to the conclusion.  $\square$

Thus, by Lemma 2.2 and the Sobolev embedding theorem [17], we obtain

**Corollary 2.1.** *The solution  $u$  of Eq. (1.1) is Hölder continuous  $u \in C^{0,1/2-\epsilon}(\Omega)$  for any small  $\epsilon > 0$ . In particular, the solution  $u \in C^0(\Omega)$ .*

Based on Lemma 2.2 and Corollary 2.1, the solution is merely in  $H^{\frac{3}{2}-\epsilon}(\Omega)$  for  $\epsilon > 0$ . The lack of regularity is largely due to the singular line Dirac measure  $\delta_\gamma$  in the source term. However, regularity is a local property. Such solution singularity shall occur only in the neighborhood of  $\gamma$ . In a large part of the domain, the solution is reasonably smooth. Hence, we shall study the regularity of Eq. (1.1) in some weighted Sobolev spaces that can accurately characterize the local behavior of the solution.

### 3. Regularity estimates in weighted spaces

Recall the domain  $\Omega$  and the line segment  $\gamma$  in Eq. (1.1). Without loss of generality, we assume  $\gamma = \{(x, 0), 0 < x < 1\}$  with the endpoints  $Q_1 = (0, 0)$  and  $Q_2 = (1, 0)$  as shown in Fig. 1. Let  $\mathcal{V}$  be the singular set, which is the collection of  $Q_1, Q_2$ , and all the vertices of  $\Omega$ . In this section, we first study an auxiliary transmission problem in Sections 3.1 and 3.2. Then, we obtain the regularity estimates for Eq. (1.1) in Section 3.3.

#### 3.1. The transmission problem

Consider the equation

$$\begin{cases} -\Delta w = 0 & \text{in } \Omega \setminus \gamma, \\ w_y^+ = w_y^- - 1 & \text{on } \gamma, \\ w^+ = w^- & \text{on } \gamma, \\ w = 0 & \text{on } \partial\Omega, \end{cases} \tag{3.1}$$

where  $w_y = \partial_y w$ . Here, for a function  $v$ ,  $v^\pm := \lim_{\epsilon \rightarrow 0} v(x, y \pm \epsilon)$ . It is clear that Eq. (3.1) has a unique weak solution

$$w \in H^1(\Omega \setminus \gamma) \cap \{w|_{\partial\Omega} = 0\}.$$

**Remark 3.1.** We define different regions of the domain as follows for further local regularity estimates. Denote by  $\mathbb{H}^+$  and  $\mathbb{H}^-$  the upper and lower half planes, respectively. Define  $\gamma_0 = \{(x, 0) : d \leq x \leq 1 - d\} \subset \gamma$  for some small  $d > 0$ . Then we choose two open subsets  $\Omega^+ \subset \Omega \cap \mathbb{H}^+$  and  $\Omega^- \subset \Omega \cap \mathbb{H}^-$ , each of whom has a smooth boundary and is away from  $\partial\Omega$ , such that  $\gamma_0 = \overline{\Omega^+} \cap \overline{\Omega^-}$ . Let  $B(x_0, r)$  be the ball centered at  $x_0$  with radius  $r$ . Denote by  $B_i = B(Q_i, 2d)$ ,  $i = 1, 2$ , the neighborhoods around the endpoints of  $\gamma$ . See Fig. 2. We assume  $d$  is sufficiently small such that  $B_1 \cap B_2 = \emptyset$  and  $(B_1 \cup B_2) \cap \partial\Omega = \emptyset$ . Therefore, the domain  $\Omega$  is divided into three regions: (i) the interior region  $R_1 = \Omega^+ \cup \Omega^-$  away from the set  $\mathcal{V}$ , (ii) the region  $R_2 = B_1 \cup B_2$  consisting of the neighborhoods of the endpoints of  $\gamma$ , and (iii)  $R_3 = \Omega \setminus (\overline{R_1} \cup \overline{R_2})$  is the region close to the boundary  $\partial\Omega$ .

**Remark 3.2.** In region  $R_3$ , the solution regularity in (3.1) is determined by the geometry of the domain. In particular, the solution can possess singularities near the non-smooth points (vertices) of the boundary. The regularity estimates in this region are well understood in the literature. See for example [18–22] and references therein. Therefore, we shall concentrate on the regularity analysis in regions  $R_1$  and  $R_2$  for Eq. (3.1).

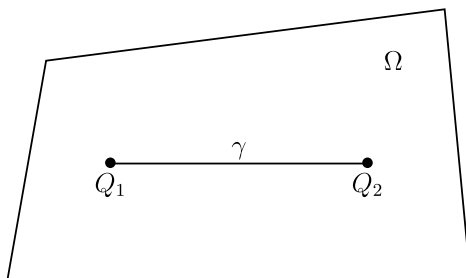


Fig. 1. Domain  $\Omega$  containing a line fracture  $\gamma$ .

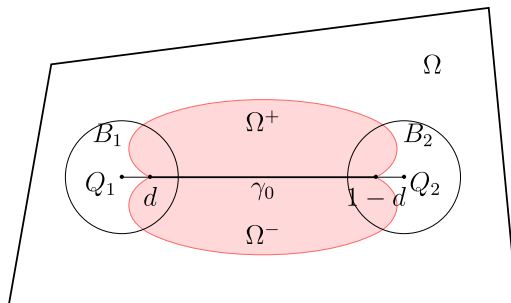


Fig. 2. Decomposition around the singular line:  $\Omega^+$ ,  $\Omega^-$ ,  $B_1$  and  $B_2$ .

We now introduce a class of Kondratiev-type weighted spaces for the analysis of Eq. (3.1).

**Definition 3.1 (Weighted Sobolev Spaces).** Recall the set  $\mathcal{V}$  that consists of the endpoints of  $\gamma$  and all the vertices of the domain  $\Omega$ . Let  $r_i(x, Q_i)$  be the distance from  $x$  to  $Q_i \in \mathcal{V}$  and let

$$\rho(x) = \prod_{Q_i \in \mathcal{V}} r_i(x, Q_i). \tag{3.2}$$

For  $a \in \mathbb{R}$ ,  $m \geq 0$ , and  $G \subset \Omega$ , we define the weighted Sobolev space

$$\mathcal{K}_a^m(G) := \{v, \rho^{|\alpha|-a} \partial^\alpha v \in L^2(G), \forall |\alpha| \leq m\},$$

where the multi-index  $\alpha = (\alpha_1, \alpha_2) \in \mathbb{Z}_{\geq 0}^2$ ,  $|\alpha| = \alpha_1 + \alpha_2$ , and  $\partial^\alpha = \partial_x^{\alpha_1} \partial_y^{\alpha_2}$ . The  $\mathcal{K}_a^m(G)$  norm for  $v$  is defined by

$$\|v\|_{\mathcal{K}_a^m(G)} = \left( \sum_{|\alpha| \leq m} \iint_G |\rho^{|\alpha|-a} \partial^\alpha v|^2 dx dy \right)^{\frac{1}{2}}.$$

**Remark 3.3.** According to Definition 3.1, in the region that is away from the set  $\mathcal{V}$ , the weighted space  $\mathcal{K}_a^m$  is equivalent to the Sobolev space  $H^m$ . In the region  $R_3$  (see Remark 3.1) that is close to the vertices of the domain, the space  $\mathcal{K}_a^m$  is the same Kondratiev space for analyzing corner singularities [19–21]. In contrast to the Kondratiev space where the weight is the distance function to the vertex set, the weight in the space  $\mathcal{K}_a^m$  also consists of the distance function to the endpoints of  $\gamma$ . In particular, for  $i = 1, 2$ , in the neighborhood  $B_i$  (Fig. 2) of an endpoint  $Q_i$  of  $\gamma$ , the weighted space can be written as

$$\mathcal{K}_a^m(B_i) = \{v, r_i^{|\alpha|-a} \partial^\alpha v \in L^2(B_i), \forall |\alpha| \leq m\}.$$

In each  $B_i$ , we further define  $\chi_i \in C_0^\infty(B_i)$  that satisfies

$$\chi_i = \begin{cases} 1 & \text{in } B(Q_i, d), \\ 0 & \text{on } \partial B_i. \end{cases}$$

Note that  $\text{supp}(\chi_1) \cap \text{supp}(\chi_2) = \emptyset$ . In addition, we denote by

$$W = \text{span}\{\chi_i\}, \quad i = 1, 2, \tag{3.3}$$

the linear span of these two functions.

### 3.2. Regularity estimates for Eq. (3.1)

We now proceed to carry out the regularity analysis for the transmission problem (3.1). Recall the interior region  $R_1 = \Omega^+ \cup \Omega^-$  in Remark 3.1. We start with the regularity analysis for the solution in  $R_1$ .

**Lemma 3.4.** *The solution of Eq. (3.1) is smooth in either  $\Omega^+$  or in  $\Omega^-$ . Namely, for any  $m \geq 1$ ,  $w \in H^{m+1}(\Omega^+)$  and  $w \in H^{m+1}(\Omega^-)$ .*

**Proof.** Recall that  $\Omega^+$  and  $\Omega^-$  are regions with a smooth boundary. Therefore, by the trace estimate, for  $m \geq 1$ , we can find two functions  $w_U \in H^{m+1}(\Omega^+)$  and  $w_D \in H^{m+1}(\Omega^-)$  such that  $w_U = w_D$  and  $\frac{\partial w_U}{\partial y} = \frac{\partial w_D}{\partial y} - 1$  on  $\gamma_0 := \overline{\Omega^+} \cap \overline{\Omega^-} \subset \gamma$ .

Define

$$w_0 = \begin{cases} w_U & \text{in } \Omega^+, \\ w_D & \text{in } \Omega^-. \end{cases}$$

Then  $w - w_0$  satisfies the standard transmission problem with a smooth interface

$$\begin{cases} -\Delta(w - w_0) = \Delta w_0 & \text{in } (\Omega^+ \cup \Omega^-), \\ (w - w_0)_y^+ = (w - w_0)_y^- & \text{on } \gamma_0, \\ (w - w_0)^+ = (w - w_0)^- & \text{on } \gamma_0. \end{cases}$$

Therefore, by the regularity results in [22,23], we have  $w - w_0 \in H^{m+1}(\Omega^+)$  and  $w - w_0 \in H^{m+1}(\Omega^-)$ , which leads to the desired result.  $\square$

We now concentrate on the solution behavior in the neighborhood  $B_i$ ,  $i = 1, 2$ , of an endpoint of  $\gamma$  (see Remark 3.1). We first consider the following problem with a simpler transmission condition on  $\gamma$ ,

$$\begin{cases} -\Delta z = f & \text{in } B_i \setminus \gamma, \\ z_y^+ = z_y^- & \text{on } \gamma \cap B_i, \\ z^+ = z^- & \text{on } \gamma \cap B_i, \\ z = 0 & \text{on } \partial B_i. \end{cases} \tag{3.4}$$

We recall a regularity result in [22] regarding  $z$  in the neighborhood of  $Q_i$ .

**Lemma 3.5.** *For Eq. (3.4), there exists  $b_{Q_i} > 0$  such that the following statement holds. Let  $0 < a < b_{Q_i}$  and  $m \geq 1$ . Assume  $f \in \mathcal{K}_{a-1}^{m-1}(B_i \setminus \gamma)$ . Recall the finite dimensional space  $W$  in (3.3). Then, there exists a unique decomposition  $z = z_{reg} + z_s$ , such that  $z_{reg} \in \mathcal{K}_{a+1}^{m+1}(B(Q_i, d) \setminus \gamma)$  and  $z_s \in W$ . Moreover, it follows*

$$\|z_{reg}\|_{\mathcal{K}_{a+1}^{m+1}(B(Q_i, d) \setminus \gamma)} + \|z_s\|_{L^\infty(B_i)} \leq C \|f\|_{\mathcal{K}_{a-1}^{m-1}(B_i \setminus \gamma)},$$

where the constant  $C > 0$  is independent of  $f$ .

**Remark 3.6.** Based on the calculation in [22], the constant  $b_{Q_i}$  is determined by the smallest positive eigenvalue of the operator  $-\partial_\theta^2$  in  $(0, 2\pi)$  with the periodic boundary condition. Note that  $k^2, k \in \mathbb{Z}_{\geq 0}$ , are these eigenvalues. Thus, it follows  $b_{Q_i} = 1$ .

Recall the solution  $w$  of the transmission problem (3.1). Recall the space  $W$  in (3.3). Then, in the neighborhood  $B_i$  of  $Q_i$ ,  $i = 1, 2$ , we have the following regularity result.

**Theorem 3.7.** *Let  $B_{d,i} := B(Q_i, d) \subset B_i$ ,  $i = 1, 2$ . Then, in  $B_{d,i}$ , the solution  $w$  of Eq. (3.1) admits a decomposition*

$$w = w_{reg} + w_s,$$

where  $w_s \in W$  and  $w_{reg} \in \mathcal{K}_{a+1}^{m+1}(B_{d,i} \setminus \gamma)$  for  $0 < a < 1$  and  $m \geq 1$ . Moreover, we have

$$\|w_{reg}\|_{\mathcal{K}_{a+1}^{m+1}(B_{d,i} \setminus \gamma)} + \|w_s\|_{L^\infty(B_i)} \leq C.$$

**Proof.** We shall derive the theorem in  $B_{d,1}$ . The proof in  $B_{d,2}$  can be carried out in a similar manner. Let  $(r, \theta)$  be the local polar coordinates in  $B_1$  for which  $Q_1$  is at the origin and  $\theta = 0$  corresponds to the positive  $x$ -axis. We shall use a localization argument to obtain the estimate. In the rest of the proof, we simplify the notation for  $B_{d,1}$  by letting  $B_d = B_{d,1}$ .

**Step 1.** Let  $\eta \in C_0^\infty(B_1)$  be a cutoff function such that  $\eta = 1$  in  $B_d$ ,  $\eta = 0$  for  $r > 3d/2$ , and  $\eta_\theta := \partial_\theta \eta = 0$ . Define  $q := \eta w$ . Note that on  $\gamma$  ( $\theta = 0, 2\pi$ ), we have

$$\begin{aligned} q_y^+ &= (\sin \theta)^+ q_r^+ + \frac{(\cos \theta)^+}{r} q_\theta^+ = \frac{1}{r} q_\theta^+ \\ &= \frac{1}{r} \eta w_\theta^+ = \eta \left( (\sin \theta)^+ w_r^+ + \frac{(\cos \theta)^+}{r} w_\theta^+ \right) = \eta w_y^+, \end{aligned}$$

where for a function  $v(r, \theta)$ ,  $v^\pm := \lim_{\epsilon \rightarrow 0} v(r, \theta \pm \epsilon)$ . With a similar calculation, we have  $q_y^- = \eta w_y^-$  on  $\gamma$ . Then, according to the transmission condition in Eq. (3.1), we have

$$q_y^+ = \eta w_y^+ = \eta(w_y^- - 1) = q_y^- - \eta, \quad \text{on } \gamma.$$

Consequently,  $q$  satisfies the following equation

$$\begin{cases} -\Delta q = -\Delta(w\eta) & \text{in } B_1 \setminus \gamma, \\ q_y^+ = q_y^- - \eta & \text{on } \gamma, \\ q^+ = q^- & \text{on } \gamma, \\ q = 0 & \text{on } \partial B_1. \end{cases} \tag{3.5}$$

Note that based on the definition of  $\eta$ , in  $B_1 \setminus \gamma$ ,  $-\Delta(w\eta) = -2\nabla w \cdot \nabla \eta - w\Delta\eta$  and in  $B_d \setminus \gamma$ ,  $-\Delta(w\eta) = 0$ .

**Step 2.** Define  $p(r, \theta) = -\eta r \sin \frac{\theta}{2}$  for  $0 \leq \theta \leq 2\pi$ , where  $\eta$  is defined in Step 1. Then  $p \in H^1(B_1)$  satisfies

$$\begin{cases} -\Delta p = \Delta \left( \eta r \sin \frac{\theta}{2} \right) & \text{in } B_1 \setminus \gamma, \\ p_y^+ = (\sin \theta)^+ p_r^+ + \frac{(\cos \theta)^+}{r} p_\theta^+ = -\frac{1}{2} \eta & \text{on } \theta = 0, \\ p_y^- = (\sin \theta)^- p_r^- + \frac{(\cos \theta)^-}{r} p_\theta^- = \frac{1}{2} \eta & \text{on } \theta = 2\pi, \\ p = 0 & \text{on } \partial B_1. \end{cases} \tag{3.6}$$

It is worth noting that  $p \notin H^2(B_1)$ . However, by a straightforward calculation, it is clear that  $p \in \mathcal{K}_{a+1}^{m+1}(B_1 \setminus \gamma)$  and  $\Delta(\eta r \sin \frac{\theta}{2}) \in \mathcal{K}_{a-1}^{m-1}(B_1 \setminus \gamma)$  for any  $m \geq 1$  and  $0 < a < 1$ .

**Step 3.** Let  $z = p - q$ . Then, based on Eqs. (3.1), (3.5), and (3.6),  $z$  satisfies

$$\begin{cases} -\Delta z = f & \text{in } B_1 \setminus \gamma, \\ z_y^+ = z_y^- & \text{on } \gamma, \\ z^+ = z^- & \text{on } \gamma, \\ z = 0 & \text{on } \partial B_1, \end{cases} \tag{3.7}$$

where  $f = \Delta(w\eta) + \Delta(\eta r \sin \frac{\theta}{2})$ . Note that by the fact  $\Delta(w\eta) = 0$  in  $B_d \setminus \gamma$  and by Lemma 3.4,  $f \in \mathcal{K}_{a-1}^{m-1}(B_1 \setminus \gamma)$  for any  $m \geq 1$  and  $0 < a < 1$ . Applying Lemma 3.5 to Eq. (3.7), we conclude that there exists a unique decomposition  $z = z_{reg} + z_s$ , with  $z_{reg} \in \mathcal{K}_{a+1}^{m+1}(B_d \setminus \gamma)$  and  $z_s \in W$ , satisfying

$$\|z_{reg}\|_{\mathcal{K}_{a+1}^{m+1}(B_d \setminus \gamma)} + \|z_s\|_{L^\infty(B_1)} \leq C \|f\|_{\mathcal{K}_{a-1}^{m-1}(B_1 \setminus \gamma)}. \tag{3.8}$$

Since  $\eta w = q = p - z$ , by the estimate (3.8) and by the definition of  $p$  in Step 2, we obtain the decomposition of  $w$  in  $B_d \setminus \gamma$ :

$$w = w_{reg} + w_s,$$

where  $w_{reg} = p - z_{reg}$  and  $w_s = -z_s$ , such that for any  $m \geq 1$  and  $0 < a < 1$ ,

$$\|w_{reg}\|_{\mathcal{K}_{a+1}^{m+1}(B_d \setminus \gamma)} + \|w_s\|_{L^\infty(B_1)} \leq C \|f\|_{\mathcal{K}_{a-1}^{m-1}(B_1 \setminus \gamma)} + \|p\|_{\mathcal{K}_{a+1}^{m+1}(B_d \setminus \gamma)} < C,$$

which completes the proof.  $\square$

### 3.3. Regularity estimates for Eq. (1.1)

Recall that  $\nu$  consists of the endpoints of  $\gamma$  and all the vertices of  $\Omega$ . Recall  $B_{d,i} := B(Q_i, d)$  in Theorem 3.7, and the regions  $\Omega^+, \Omega^-, R_3$  in Remark 3.1. We are now ready to derive the regularity estimate for the solution of Eq. (1.1) with the line Dirac measure.

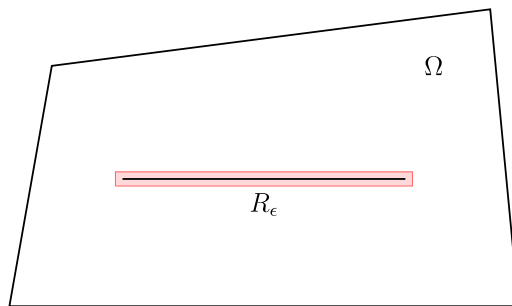


Fig. 3. A small neighborhood  $R_\epsilon$  of the line fracture  $\gamma$ .

**Theorem 3.8.** The solution  $u$  of Eq. (1.1) is smooth in the region away from the set  $\gamma$ , namely, for  $m \geq 1$ ,  $u \in H^{m+1}(\Omega^+)$  and  $u \in H^{m+1}(\Omega^-)$ . In the neighborhood of each endpoint of  $\gamma$ ,  $u$  admits a decomposition

$$u = u_{reg} + u_s, \quad u_s \in W,$$

such that for any  $m \geq 1$  and  $0 < a < 1$ ,

$$\|u_{reg}\|_{\mathcal{K}_{a+1}^{m+1}(B_{d,i} \setminus \gamma)} + \|u_s\|_{L^\infty(B_i)} \leq C.$$

In the region  $R_3$  away from  $\gamma$  and close to the boundary,  $u \in \mathcal{K}_{a+1}^{m+1}(R_3)$  for  $m \geq 1$  and  $0 < a < \frac{\pi}{\omega}$ , where  $\omega$  is the largest interior angle among all the vertices of the domain  $\Omega$ .

**Proof.** Recall the solution  $w$  of the transmission problem (3.1). We shall show  $u = w$ . We first extend  $w$  to  $\Omega$  by defining

$$w := \begin{cases} w & \text{in } \Omega \setminus \gamma, \\ w^+ (= w^-) & \text{on } \gamma. \end{cases}$$

For  $\epsilon > 0$  small, define  $R_\epsilon := \{(-\epsilon, 1 + \epsilon) \times (-\epsilon, \epsilon)\}$  to be a small neighborhood of  $\gamma$ . Let  $\mathbf{n}_\epsilon$  be the unit outward normal vector to  $\partial R_\epsilon$ . See Fig. 3. Let  $\tilde{u} = u - w$ . Then for any  $\phi \in C_0^\infty(\Omega)$ , it follows

$$\begin{aligned} - \iint_{\Omega} \Delta \tilde{u} \phi dx dy &= - \iint_{\Omega} \Delta u \phi dx dy + \iint_{\Omega} \Delta w \phi dx dy \\ &= \iint_{\Omega} \delta_\gamma \phi dx dy + \iint_{\Omega \setminus R_\epsilon} \Delta w \phi dx dy + \iint_{R_\epsilon} \Delta w \phi dx dy \\ &= \int_{\gamma} \phi ds + \iint_{\Omega \setminus R_\epsilon} \Delta w \phi dx dy - \iint_{R_\epsilon} \nabla w \cdot \nabla \phi dx dy + \int_{\partial R_\epsilon} \nabla w \cdot \mathbf{n}_\epsilon \phi ds. \end{aligned} \tag{3.9}$$

For each term on the right hand side of (3.9), we have the following estimates. In particular,

$$\int_{\partial R_\epsilon} \nabla w \cdot \mathbf{n}_\epsilon \phi ds = \int_{-\epsilon}^{1+\epsilon} (w_y(x, \epsilon) - w_y(x, -\epsilon)) \phi dx + \int_{-\epsilon}^{\epsilon} (w_x(1 + \epsilon, y) - w_x(-\epsilon, y)) \phi dy.$$

By (3.1) we have

$$\iint_{\Omega \setminus R_\epsilon} \Delta w \phi dx dy = 0.$$

As  $\epsilon \rightarrow 0$ , due to the boundedness of  $|\nabla w|$  in  $R_\epsilon$ , it follows

$$\iint_{R_\epsilon} \nabla w \cdot \nabla \phi dx dy \rightarrow 0;$$

and by the transmission condition in (3.1), we further have

$$\int_{\partial R_\epsilon} \nabla w \cdot \mathbf{n}_\epsilon \phi ds \rightarrow \int_0^1 (w_y(x, 0+) - w_y(x, 0-)) \phi dx = - \int_{\gamma} \phi dx.$$

Incorporating the above estimates into (3.9), we have

$$- \iint_{\Omega} \Delta \tilde{u} \phi dx dy = 0, \quad \forall \phi \in C_0^\infty(\Omega).$$



Fig. 4. The new node of the edge  $pq$  (left–right): no singular vertices (midpoint);  $p$  is a singular point ( $|pr| = \kappa_p|pq|$ ,  $\kappa_p < 0.5$ ).

We then conclude that

$$-\Delta \tilde{u} = 0 \quad \text{in } \Omega.$$

Note that  $\tilde{u} = u - w = 0$  on  $\partial\Omega$ , then it follows  $\tilde{u} = 0$  in  $\Omega$ , namely,  $u = w$  in  $\Omega$ .

Therefore, the regularity estimates for  $u$  in  $\Omega^+$ ,  $\Omega^-$ , and in  $B_{d_i}$ ,  $i = 1, 2$  can be derived from the corresponding estimates for  $w$  in Lemma 3.4 and in Theorem 3.7. The regularity estimates for  $u$  in  $R_3$  follow from the results in [20,21] for elliptic Dirichlet problems in polygonal domains.  $\square$

#### 4. Optimal finite element methods

According to Lemma 2.2, the solution of Eq. (1.1) is merely in  $H^{\frac{3}{2}-\epsilon}(\Omega)$  for any  $\epsilon > 0$ . The singularities in the solution can severely slow down the convergence of the usual finite element method associated with a quasi-uniform mesh. In this section, we propose new finite element algorithms to approximate the solution of Eq. (1.1) that shall converge at the optimal rate.

##### 4.1. The finite element method

Let  $\mathcal{T} = \{T_i\}$  be a triangulation of  $\Omega$  with triangles. For  $m \geq 1$ , we denote the Lagrange finite element space by

$$S(\mathcal{T}, m) = \{v \in C^0(\Omega) \cap H_0^1(\Omega) : v|_T \in P_m(T), \forall T \in \mathcal{T}\},$$

where  $P_m(T)$  is the space of polynomials with degree no more than  $m$  on  $T$ . Following the variational form (2.1), we define the finite element solution  $u_h \in S(\mathcal{T}, m)$  of Eq. (1.1) by

$$\int_{\Omega} \nabla u_h \cdot \nabla v_h dx = \int_{\gamma} v_h dx, \quad \forall v_h \in S(\mathcal{T}, m).$$

Suppose that the mesh  $\mathcal{T}$  consists of quasi-uniform triangles with size  $h$ . Because of the lack of regularity in the solution ( $u \in H^{\frac{3}{2}-\epsilon}(\Omega)$ ), the standard error estimate [17] yields only a sup-optimal convergence rate

$$\|u - u_h\|_{H^1(\Omega)} \leq Ch^{\frac{1}{2}-\epsilon}, \quad \text{for } \epsilon > 0.$$

This is highly ineffective since the optimal convergence rate using the  $m$ th-degree polynomials when the solution is smooth is

$$\|u - u_h\|_{H^1(\Omega)} \leq Ch^m.$$

We now propose new finite element methods to solve equation (1.1) based on the special refinement of the triangles. Recall that the singular set  $\mathcal{V}$  includes the endpoints of  $\gamma$  and all the vertices of  $\Omega$ . We call the points in  $\mathcal{V}$  the *singular points*.

**Algorithm 4.1 (Graded Refinements).** Suppose each singular point is a vertex in the triangulation  $\mathcal{T}$  and each triangle in  $\mathcal{T}$  contains at most one singular point. We also suppose  $\mathcal{T}$  conforms to  $\gamma$ . Namely,  $\gamma$  is the union of some edges in  $\mathcal{T}$  and does not cross triangles in  $\mathcal{T}$ . Let  $pq$  be an edge in the triangulation  $\mathcal{T}$  with  $p$  and  $q$  as the endpoints. Then, in a graded refinement, a new node  $r$  on  $pq$  is produced according to the following conditions:

1. (Neither  $p$  or  $q$  is a singular point.) We choose  $r$  as the midpoint ( $|pr| = |qr|$ ).
2. ( $p$  is a singular point.) We choose  $r$  such that  $|pr| = \kappa_p|pq|$ , where  $\kappa_p \in (0, 0.5)$  is a parameter that will be specified later. See Fig. 4 for example.

Then, the graded refinement, denoted by  $\kappa(\mathcal{T})$ , proceeds as follows. For each triangle in  $\mathcal{T}$ , a new node is generated on each edge as described above. Then,  $T$  is decomposed into four small triangles by connecting these new nodes (Fig. 5). Given an initial mesh  $\mathcal{T}_0$  satisfying the condition above, the associated family of graded meshes  $\{\mathcal{T}_n, n \geq 0\}$  is defined recursively  $\mathcal{T}_{n+1} = \kappa(\mathcal{T}_n)$ .

**Remark 4.2.** In Algorithm 4.1, we choose the parameter  $\kappa_p$  for each  $p \in \mathcal{V}$  as follows. Recall  $m$  is the degree of polynomials in the finite element space  $S(\mathcal{T}_n, m)$ . Then, if  $p$  is an endpoint of  $\gamma$ , we choose  $\kappa_p = 2^{-\frac{m}{a}}$  for any  $0 < a < 1$ , and if  $p$  is a vertex of the domain  $\Omega$ , we choose  $\kappa_p < 2^{-\frac{m\omega}{\pi}}$ , where  $\omega$  is the largest interior angle of the domain.



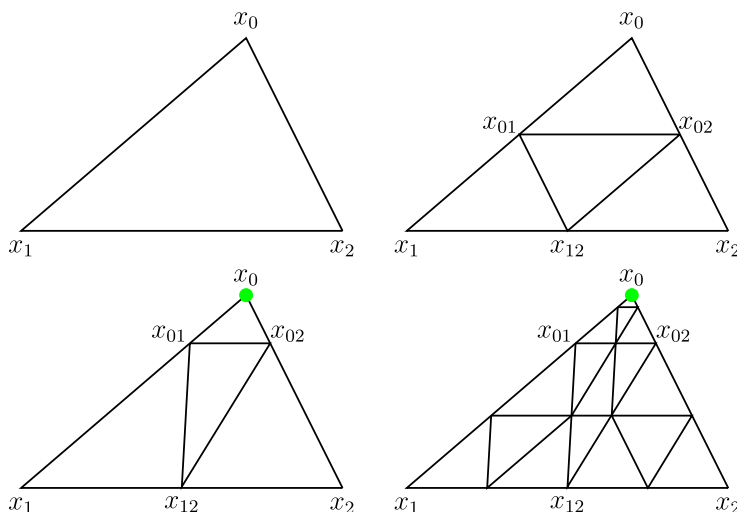


Fig. 5. Refinement of a triangle  $\Delta x_0x_1x_2$ . First row: (left–right): the initial triangle and the midpoint refinement; second row: two consecutive graded refinements toward  $x_0 = Q$ . ( $\kappa < 0.5$ ).

Let  $S_n := S(\mathcal{T}_n, m)$  be the finite element space of degree  $m$  associated with the graded meshes defined in Algorithm 4.1 and Remark 4.2. Then, we define the finite element solution  $u_n \in S_n$  as

$$a(u_n, v_n) = \int_{\Omega} \nabla u_n \cdot \nabla v_n dx = \int_{\gamma} v_n dx, \quad \forall v_n \in S_n. \tag{4.1}$$

Note that the bilinear form  $a(\cdot, \cdot)$  is coercive and continuous on  $S_n$ . Thus, by C ea’s Theorem, we have

$$\|u - u_n\|_{H^1(\Omega)} \leq C \inf_{v \in S_n} \|u - v\|_{H^1(\Omega)}. \tag{4.2}$$

In the rest of this section, we shall show that the proposed numerical solution  $u_n$  converges to the solution  $u$  of (1.1) in the optimal rate.

#### 4.2. Interpolation error estimates

Recall the three regions  $R_1, R_2$  and  $R_3$  of the domain  $\Omega$  in Remark 3.1.  $R_1$  is the region that is away from the singular set  $\mathcal{V}$ .  $R_2$  is the region close to the endpoints of  $\gamma$  and  $R_3$  is the region close to the boundary of the domain. According to the regularity analysis in Section 3, the solution of Eq. (1.1) behaves differently in these three regions. We therefore focus on the local interpolation error analysis in different regions.

##### 4.2.1. Interpolation error estimates in $R_1$ and $R_3$

**Lemma 4.3.** Recall the triangulation  $\mathcal{T}_n$  in Algorithm 4.1 and Remark 4.2. Let  $T_{(0)} \in \mathcal{T}_0$  be an initial triangle and let  $u_I$  be the nodal interpolation of  $u$  associated with  $\mathcal{T}_n$ . If  $\bar{T}_{(0)}$  does not contain the endpoint of  $\gamma$ , then

$$\|u - u_I\|_{H^1(T_{(0)})} \leq Ch^m,$$

where  $h := 2^{-n}$ .

**Proof.** Note that if  $\bar{T}_0$  does not contain the endpoint of  $\gamma$ , then  $\bar{T}_{(0)} \cap \mathcal{V} = \emptyset$  or  $\bar{T}_{(0)}$  contains a vertex of the domain  $\Omega$ . If  $\bar{T}_{(0)} \cap \mathcal{V} = \emptyset$ , we have  $u \in H^{m+1}(T_{(0)})$  (Theorem 3.8) and the mesh on  $T_{(0)}$  is quasi-uniform (Algorithm 4.1) with size  $O(2^{-n})$ . Therefore, based on the standard interpolation error estimate, we have

$$\|u - u_I\|_{H^1(T_{(0)})} \leq Ch^m \|u\|_{H^{m+1}(T_{(0)})} \leq Ch^m. \tag{4.3}$$

In the case that  $\bar{T}_0$  contains a vertex of the domain, the solution may be singular in the neighborhood of a corner. Based on the results in [24], the solution  $u \in \mathcal{K}_{a+1}^{m+1}(T_{(0)})$  for  $a < \frac{\pi}{\omega}$  and  $m \geq 1$ , where  $\omega$  is the largest interior angle of the domain. Note that the graded mesh on  $T_{(0)}$  with the parameter in Remark 4.2 is the same mesh defined in [22,24], which can recover the optimal convergence rate in the finite element method even when the solution has corner singularities:

$$\|u - u_I\|_{H^1(T_{(0)})} \leq Ch^m. \tag{4.4}$$

The proof is hence completed by (4.3) and (4.4).  $\square$

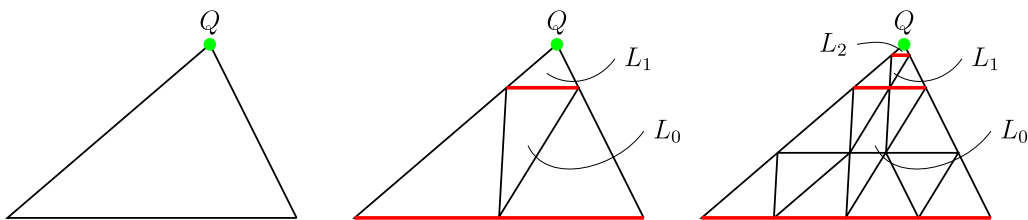


Fig. 6. Mesh layers (left-right): the initial triangle  $T_{(0)}$  with a vertex  $Q$ ; two layers after one refinement; three layers after two refinements.

4.2.2. Interpolation error estimates in  $R_2$

We now study the interpolation error in the neighborhood of the endpoint  $Q$  of  $\gamma$ . In the rest of this subsection, we assume  $T_{(0)} \in \mathcal{T}_0$  is an initial triangle such that  $Q$  is a vertex of  $T$ . According to Remark 4.2, the mesh on  $T_{(0)}$  is graded toward  $Q$  with  $\kappa_Q = 2^{-\frac{m}{a}}$  for any  $0 < a < 1$ . We first define mesh layers on  $T_0$  which are collections of triangles in  $\mathcal{T}_n$ .

**Definition 4.1 (Mesh Layers).** Let  $T_{(i)} \subset T_{(0)}$  be the triangle in  $\mathcal{T}_i$ ,  $0 \leq i \leq n$ , that is attached to the singular vertex  $Q$  of  $T_{(0)}$ . For  $0 \leq i < n$ , we define the  $i$ th mesh layer of  $\mathcal{T}_n$  on  $T_{(0)}$  to be the region  $L_i := T_{(i)} \setminus T_{(i+1)}$ ; and for  $i = n$ , the  $n$ th layer is  $L_n := T_{(n)}$ . See Fig. 6 for example.

**Remark 4.4.** The triangles in  $\mathcal{T}_n$  constitute  $n$  mesh layers on  $T_{(0)}$ . According to Algorithm 4.1 and the choice of grading parameters in Remark 4.2, the mesh size in the  $i$ th layer  $L_i$  is

$$O(\kappa_Q^i 2^{i-n}). \tag{4.5}$$

Meanwhile, the weight function  $\rho$  in (3.2) satisfies

$$\rho = O(\kappa_Q^i) \text{ in } L_i \text{ (} 0 \leq i < n \text{)} \quad \text{and} \quad \rho \leq C\kappa_Q^n \text{ in } L_n. \tag{4.6}$$

Although the mesh size varies in different layers, the triangles in  $\mathcal{T}_n$  are shape regular. In addition, using the local Cartesian coordinates such that  $Q$  is the origin, the mapping

$$\mathbf{B}_i = \begin{pmatrix} \kappa_Q^{-i} & 0 \\ 0 & \kappa_Q^{-i} \end{pmatrix}, \quad 0 \leq i \leq n \tag{4.7}$$

is a bijection between  $L_i$  and  $L_0$  for  $0 \leq i < n$  and a bijection between  $L_n$  and  $T_{(0)}$ . We call  $L_0$  (resp.  $T_{(0)}$ ) the reference region associated to  $L_i$  for  $0 \leq i < n$  (resp.  $L_n$ ).

With the mapping (4.7), we have that for any point  $(x, y) \in L_i$ ,  $0 \leq i \leq n$ , the image point  $(\hat{x}, \hat{y}) := \mathbf{B}_i(x, y)$  is in its reference region. Moreover, we have the following dilation result.

**Lemma 4.5.** For  $0 \leq i \leq n$ , given a function  $v(x, y) \in \mathcal{K}_a^l(L_i)$ , the function  $\hat{v}(\hat{x}, \hat{y}) := v(x, y)$  belongs to  $\mathcal{K}_a^l(\hat{L})$ , where  $(\hat{x}, \hat{y}) := \mathbf{B}_i(x, y)$ ,  $\hat{L} = L_0$  for  $0 \leq i < n$ , and  $\hat{L} = T_{(0)}$  for  $i = n$ . Moreover, it follows

$$\|\hat{v}(\hat{x}, \hat{y})\|_{\mathcal{K}_a^l(\hat{L})} = \kappa_Q^{i(a-1)} \|v(x, y)\|_{\mathcal{K}_a^l(L_i)}.$$

**Proof.** Let  $r$  be the distance from  $(x, y)$  to  $Q$ , then the distance from  $(\hat{x}, \hat{y})$  to  $Q$  is  $\hat{r} = \kappa_Q^{-i}r$ . By definition, we have

$$\begin{aligned} \|\hat{v}(\hat{x}, \hat{y})\|_{\mathcal{K}_a^l(\hat{L})}^2 &= \sum_{j+k \leq l} \int_{\hat{L}} |\hat{r}^{j+k-a} \partial_{\hat{x}}^j \partial_{\hat{y}}^k \hat{v}|^2 d\hat{x}d\hat{y} \\ &= \sum_{j+k \leq l} \int_{L_i} |\kappa_Q^{-i(j+k-a)} r^{j+k-a} \kappa_Q^{i(j+k)} \partial_x^j \partial_y^k v|^2 \kappa_Q^{-2i} dx dy \\ &= \kappa_Q^{i(2a-2)} \sum_{j+k \leq l} \int_{L_i} |r^{j+k-a} \partial_x^j \partial_y^k v|^2 dx dy = \kappa_Q^{i(2a-2)} \|v\|_{\mathcal{K}_a^l(L_i)}^2, \end{aligned}$$

which completes the proof.  $\square$

We then derive the interpolation error estimate in each layer.

**Lemma 4.6.** Recall  $\kappa_Q = 2^{-\frac{m}{a}}$  for the graded mesh on  $T_{(0)}$ ,  $m \geq 1$  and  $0 < a < 1$ . Let  $u_I$  be the nodal interpolation of  $u$  in the  $i$ th layer  $L_i$  on  $T_{(0)}$ ,  $0 \leq i < n$ . Then, for  $h := 2^{-n}$ , we have

$$\|u - u_I\|_{H^1(L_i)} \leq Ch^m.$$

**Proof.** Based on [Theorem 3.8](#), the solution can be decomposed into two parts on  $T_{(0)}$ ,  $u = u_{reg} + u_s$ , where for  $m \geq 1$  and  $0 < a < 1$ ,

$$\|u_{reg}\|_{\mathcal{K}_{a+1}^{m+1}(T_{(0)})} + \|u_s\|_{L^\infty(T_{(0)})} \leq C.$$

Since  $u_s \in W$  is smooth and belongs to a finite dimensional space, the norms of  $u_s$  are equivalent. Thus, we have

$$\|u_{reg}\|_{\mathcal{K}_{a+1}^{m+1}(T_{(0)})} + \|u_s\|_{H^{m+1}(T_{(0)})} \leq C. \tag{4.8}$$

Note that in each  $L_i$ ,  $i < n$ , the space  $\mathcal{K}_{a+1}^{m+1}$  is equivalent to  $H^{m+1}$ . Therefore, both  $u_{reg}$  and  $u_s$  are continuous functions in  $L_i$ . Let  $u_{reg,l}$  and  $u_{s,l}$  be the nodal interpolations of  $u_{reg}$  and  $u_s$ , respectively. Then, it is clear that  $u_l = u_{reg,l} + u_{s,l}$ . Thus, we have

$$|u - u_l|_{H^1(L_i)} \leq |u_{reg} - u_{reg,l}|_{H^1(L_i)} + |u_s - u_{s,l}|_{H^1(L_i)}. \tag{4.9}$$

We shall obtain the estimate for each term on the right hand side of [\(4.9\)](#).

Recall the mapping  $\mathbf{B}_i$  in [\(4.7\)](#). For any point  $(x, y) \in L_i$ , let  $(\hat{x}, \hat{y}) = \mathbf{B}_i(x, y) \in L_0$ . Then, for a function  $v(x, y)$  in  $L_i$ , define  $\hat{v}(\hat{x}, \hat{y}) := v(x, y)$  in  $L_0$ . Using the standard interpolation error estimate, the scaling argument, the estimate in [\(4.5\)](#), and the mapping in [\(4.7\)](#), we have

$$\begin{aligned} |u_{reg} - u_{reg,l}|_{H^1(L_i)} &= |\hat{u}_{reg} - \hat{u}_{reg,l}|_{H^1(L_0)} \leq C2^{(i-n)m} |\hat{u}_{reg}|_{H^{m+1}(L_0)} \\ &\leq C2^{(i-n)m} \kappa_Q^{mi} |u_{reg}|_{H^{m+1}(L_i)} = Ch^m (2\kappa_Q)^{mi} |u_{reg}|_{H^{m+1}(L_i)}. \end{aligned}$$

Recall  $\kappa_Q < 2^{-\frac{m}{a}}$  for any  $0 < a < 1$  and recall the estimate in [\(4.6\)](#). Then, continuing the estimate above, we obtain

$$\begin{aligned} |u_{reg} - u_{reg,l}|_{H^1(L_i)}^2 &\leq Ch^{2m} \sum_{|\alpha|=m+1} |\rho^{-1-a} \rho^{m+1} \partial^\alpha u_{reg}|_{L^2(L_i)}^2 \\ &\leq Ch^{2m} \|u_{reg}\|_{\mathcal{K}_{a+1}^{m+1}(L_i)}^2, \end{aligned} \tag{4.10}$$

where the last step is based on definition of the weighted space.

For  $|u_s - u_{s,l}|_{H^1(L_i)}$ , by the fact that  $\kappa_Q < 0.5$ , we similarly have

$$\begin{aligned} |u_s - u_{s,l}|_{H^1(L_i)} &= |\hat{u}_s - \hat{u}_{s,l}|_{H^1(L_0)} \leq C2^{(i-n)m} |\hat{u}_s|_{H^{m+1}(L_0)} \\ &\leq C2^{(i-n)m} \kappa_Q^{mi} |u_s|_{H^{m+1}(L_i)} = Ch^m |u_s|_{H^{m+1}(L_i)}. \end{aligned} \tag{4.11}$$

Then, the proof is completed by combining [\(4.9\)](#), [\(4.10\)](#), [\(4.11\)](#), and [\(4.8\)](#).  $\square$

We now derive the interpolation error estimate in the last layer  $L_n$  on  $T_{(0)}$ .

**Lemma 4.7.** Recall  $\kappa_Q = 2^{-\frac{m}{a}}$  for the graded mesh on  $T_{(0)}$ ,  $m \geq 1$  and  $0 < a < 1$ . Let  $u_l$  be the nodal interpolation of  $u$  in the  $n$ th layer  $L_n$  on  $T_{(0)}$  for  $n$  sufficiently large. Then, for  $h := 2^{-n}$ , we have

$$|u - u_l|_{H^1(L_n)} \leq Ch^m.$$

**Proof.** Recall from [Theorem 3.8](#) that on  $T_{(0)}$ ,  $u = u_{reg} + u_s \in \mathcal{K}_{a+1}^{m+1} + W$  (see also [\(4.8\)](#)). Let  $u_{reg,l}$  and  $u_{s,l}$  be the nodal interpolations of  $u_{reg}$  and  $u_s$ , respectively. Recall  $u_s$  is a constant in the  $n$ th layer  $L_n$  when  $n$  is sufficiently large, and therefore  $(u_s - u_{s,l})_{L_n} = 0$ . Thus, it is sufficient to estimate  $|u_{reg} - u_{reg,l}|_{H^1(L_n)}$ .

Recall the mapping  $\mathbf{B}_n$  in [\(4.7\)](#). For any point  $(x, y) \in L_n$ , let  $(\hat{x}, \hat{y}) = \mathbf{B}_n(x, y) \in T_{(0)}$ . Then, for a function  $v(x, y)$  in  $L_n$ , define  $\hat{v}(\hat{x}, \hat{y}) := v(x, y)$  in  $T_{(0)}$ . Let  $\psi : T_{(0)} \rightarrow [0, 1]$  be a smooth function that is equal to 0 in a neighborhood of  $Q$ , but is equal to 1 at all the other nodal points in  $\mathcal{T}_0$ . Then, we let  $w = \psi \hat{u}_{reg}$  in  $T_{(0)}$ . Consequently, we have for  $l \geq 0$

$$\|w\|_{\mathcal{K}_1^l(T_{(0)})}^2 = \|\psi \hat{u}_{reg}\|_{\mathcal{K}_1^l(T_{(0)})}^2 \leq C \|\hat{u}_{reg}\|_{\mathcal{K}_1^l(T_{(0)})}^2, \tag{4.12}$$

where  $C$  depends on  $l$  and the smooth function  $\psi$ . Moreover, the condition  $\hat{u}_{reg} \in \mathcal{K}_{a+1}^{m+1}(T_{(0)})$  with  $a > 0$  and  $m \geq 1$  implies  $\hat{u}_{reg}(Q) = 0$  (see, e.g., [\[25, Lemma 4.7\]](#)). Let  $w_l$  be the nodal interpolation of  $w$  associated with the mesh  $\mathcal{T}_0$  on  $T_{(0)}$ . Therefore, by the definition of  $w$ , we have

$$w_l = \hat{u}_{reg,l} = \widehat{u_{reg,l}} \quad \text{in } T_{(0)}. \tag{4.13}$$

Note that the  $\mathcal{K}_1^l$  norm and the  $H^l$  norm are equivalent for  $w$  on  $T_{(0)}$ , since  $w = 0$  in the neighborhood of the vertex  $Q$ . Let  $r$  be the distance from  $(x, y)$  to  $Q$ , and  $\hat{r}$  be the distance from  $(\hat{x}, \hat{y})$  to  $Q$ . Then, by the definition of the weighted

space, the scaling argument, (4.12), (4.13), and (4.6), we have

$$\begin{aligned}
 \|u_{reg} - u_{reg,I}\|_{H^1(L_n)}^2 &\leq C \|u_{reg} - u_{reg,I}\|_{\mathcal{K}_1^1(L_n)}^2 \leq C \sum_{|\alpha| \leq 1} \|r(x, y)^{|\alpha|-1} \partial^\alpha (u_{reg} - u_{reg,I})\|_{L^2(L_n)}^2 \\
 &= C \sum_{|\alpha| \leq 1} \|\hat{r}(\hat{x}, \hat{y})^{|\alpha|-1} \partial^\alpha (\hat{u}_{reg} - \widehat{u_{reg,I}})\|_{L^2(T_{(0)})}^2 \leq C \|\hat{u}_{reg} - w + w - \widehat{u_{reg,I}}\|_{\mathcal{K}_1^1(T_{(0)})}^2 \\
 &\leq C (\|\hat{u}_{reg} - w\|_{\mathcal{K}_1^1(T_{(0)})}^2 + \|w - \widehat{u_{reg,I}}\|_{\mathcal{K}_1^1(T_{(0)})}^2) \\
 &= C (\|\hat{u}_{reg} - w\|_{\mathcal{K}_1^1(T_{(0)})}^2 + \|w - w_j\|_{\mathcal{K}_1^1(T_{(0)})}^2) \\
 &\leq C (\|\hat{u}_{reg}\|_{\mathcal{K}_1^1(T_{(0)})}^2 + \|w\|_{\mathcal{K}_1^{m+1}(T_{(0)})}^2) \leq C (\|\hat{u}_{reg}\|_{\mathcal{K}_1^1(T_{(0)})}^2 + \|\hat{u}_{reg}\|_{\mathcal{K}_1^{m+1}(T_{(0)})}^2) \\
 &= C (\|u_{reg}\|_{\mathcal{K}_1^1(L_n)}^2 + \|u_{reg}\|_{\mathcal{K}_1^{m+1}(L_n)}^2) \leq C \kappa_Q^{2na} \|u_{reg}\|_{\mathcal{K}_{a+1}^{m+1}(L_n)}^2 \\
 &\leq C 2^{-2nm} \|u_{reg}\|_{\mathcal{K}_{a+1}^{m+1}(L_n)}^2 \leq Ch^{2m},
 \end{aligned}$$

where the ninth relationship is based on Lemma 4.5. This completes the proof.  $\square$

Therefore, for the finite element method solving equation (1.1) defined in Algorithm 4.1 and Remark 4.2, we obtain the optimal convergence rate.

**Theorem 4.8.** Let  $S_n$  be the finite element space associated with the graded triangulation  $\mathcal{T}_n$  defined in Algorithm 4.1 and Remark 4.2. Let  $u_n \in S_n$  be the finite element solution of Eq. (1.1) defined in (4.1). Then,

$$\|u - u_n\|_{H^1(\Omega)} \leq Ch^m \leq C \dim(S_n)^{-\frac{m}{2}},$$

where  $h := 2^{-n}$  and  $\dim(S_n)$  is the dimension of  $S_n$ .

**Proof.** By Céa’s Theorem (see (4.2)),

$$\|u - u_n\|_{H^1(\Omega)}^2 \leq C \|u - u_I\|_{H^1(\Omega)}^2 = C \sum_{T_{(0)} \in \mathcal{T}_0} \|u - u_I\|_{H^1(T_{(0)})}^2.$$

Based on the Poincaré inequality and Lemmas 4.6 and 4.7, if the initial triangle  $T_{(0)}$  has an endpoint of  $\gamma$  as a vertex, we have

$$\|u - u_I\|_{H^1(T_{(0)})}^2 \leq Ch^{2m} = C 2^{-2mn}.$$

Summing up this estimate and the estimates in Lemma 4.3, and noting that based on Algorithm 4.1  $\dim S_n = O(4^n)$ , we obtain

$$\|u - u_n\|_{H^1(\Omega)}^2 \leq Ch^{2m} \leq C \dim(S_n)^{-m},$$

which completes the proof.  $\square$

**Remark 4.9.** The solution of Eq. (1.1) may possess singularities across the line segment  $\gamma$ , near the vertices of the domain, and near the endpoints of  $\gamma$ . We have derived regularity results in weighted Sobolev spaces and proposed numerical methods that solve equation (1.1) in the optimal convergence rate. These results can be extended to more general cases, for example, the case where the line fracture is replaced by multiple line fractures, whether intersecting or non-intersecting. With proper modifications, we also expect the analytical tools will be useful when  $\gamma$  is a smooth curve and when the source term  $\delta_\gamma$  is replaced by  $q\delta_\gamma$  for  $q \in L^2(\gamma)$ .

### 5. Numerical examples

In this section, we present numerical test results to validate our theoretical predictions for the proposed finite element method solving equation (1.1). Since the solution  $u$  is unknown, we use the following numerical convergence rate

$$e = \log_2 \frac{|u_j - u_{j-1}|_{H^1(\Omega)}}{|u_{j+1} - u_j|_{H^1(\Omega)}}, \tag{5.1}$$

where  $u_j$  is the finite element solution on the mesh  $\mathcal{T}_j$  obtained after  $j$  refinements of the initial triangulation  $\mathcal{T}_0$ . According to Theorem 4.8, when the optimal convergence rate is obtained, the value of  $e$  shall be close to  $m$ , where  $m$  is the degree of the polynomial used in the numerical method. This desired rate can be achieved especially when the grading parameter near the endpoint  $Q$  of  $\gamma$  satisfies  $\kappa_Q = 2^{-\frac{m}{a}}$  for any  $0 < a < 1$  and the grading parameter near a vertex  $p$  of domain satisfies  $\kappa_p < 2^{-\frac{m\omega}{\pi}}$ , where  $\omega$  is the largest interior angle among all the vertices of  $\Omega$ .

For Examples 5.1 and 5.2, we consider the finite element method based on  $P_1$  polynomials for problem (1.1) in a square domain  $\Omega = (0, 1)^2$ .

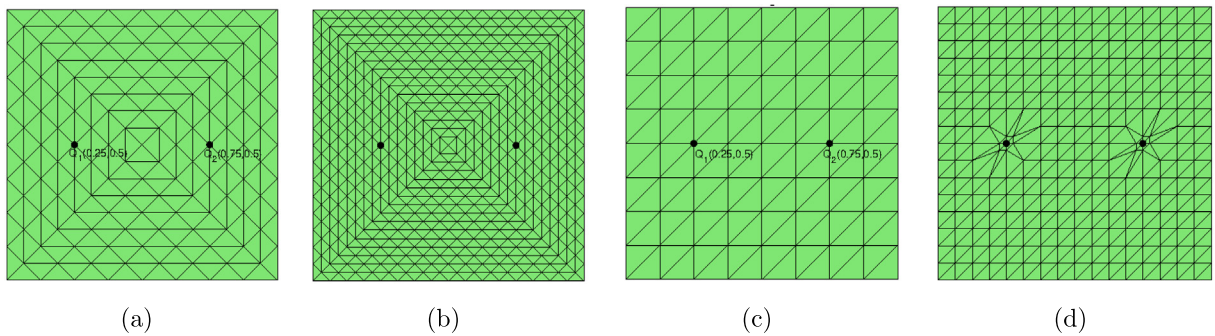


**Fig. 7.** Graded mesh and Union-Jack mesh. (a) and (b): the initial Union-Jack mesh and the mesh after one refinement. (c) and (d): the initial graded mesh and the mesh after one refinement,  $\kappa = \kappa_{Q_1} = \kappa_{Q_2} = 0.2$ .

**Table 1**  
Convergence history of the numerical solution in Example 5.1 with mesh refinements.

$\kappa \setminus j$	$j = 2$	$j = 3$	$j = 4$	$j = 5$
$\kappa = 0.1$	0.99	0.94	0.97	0.99
$\kappa = 0.2$	0.97	0.99	0.99	1.00
$\kappa = 0.3$	0.87	0.96	0.99	1.00
$\kappa = 0.4$	0.86	0.91	0.94	0.98
$\kappa = 0.5$	0.84	0.87	0.89	0.91
Union-Jack	0.46	0.47	0.49	0.49

**Example 5.1 (Union-Jack Meshes and Graded Meshes).** In this example, the line fracture  $\gamma = Q_1Q_2$  has two vertices  $Q_1 = (0.25, 0.5)$  and  $Q_2 = (0.75, 0.5)$ . We use finite element methods on two types of triangular meshes: the Union-Jack mesh with elements across the line fracture  $\gamma$ ; and the graded meshes conforming to  $\gamma$  defined in Algorithm 4.1 with different values of the grading parameter. The initial triangulations are given in (a) and (c) of Fig. 7, respectively, where the Union-Jack mesh has 128 elements and the graded mesh has 64 elements. To refine the Union-Jack mesh, each triangle is divided into four equal triangles.

Note that in the square domain, the vertices of the domain do not lead to corner singularities in  $H^2$ . Therefore, we use quasi-uniform meshes near the corners, which shall not affect the global convergence rate. However, in the region across  $\gamma$ , the solution merely belongs to  $H^{\frac{3}{2}-\epsilon}$  for any  $\epsilon > 0$ . Union-Jack mesh does not resolve the singularity across the fracture  $\gamma$ . Thus, on the Union-Jack mesh, the convergence rate (5.1) of the numerical solution shall be about 0.5. The graded mesh conforms to  $\gamma$  and therefore resolves the solution singularity across  $\gamma$ . Based on Theorem 4.8, when the grading parameter for the endpoints of  $\gamma$  satisfies  $\kappa := \kappa_{Q_1} = \kappa_{Q_2} = 2^{-\frac{1}{\alpha}} < 0.5$ , the singular solution near  $Q_1$  and  $Q_2$  shall be well approximated, which yields the optimal convergence rate in the numerical approximation.

The convergence rates (5.1) associated with these two types of meshes are reported in Table 1. The first five rows are the rates on graded meshes, and the last row contains data on the Union-Jack mesh. Here  $j$  is the number of refinements from the initial mesh. It is clear that the rate on a sequence of Union-Jack meshes is suboptimal with  $e = 0.5$ . For graded meshes, when  $\kappa < 0.5$ , the convergence rate is optimal with rate  $e = 1$ ; and the convergence is not optimal when  $\kappa = 0.5$ . These results are closely aligned with our aforementioned theoretical predication.

**Example 5.2 (Graded Meshes for Different Fractures).** This example is to test the convergence rate on a sequence of graded meshes for problem (1.1) with the line fracture(s) at different locations. We shall use the linear finite element method and the same square domain as in Example 5.1 for all the numerical tests in this example.

**Test 1.** Suppose we have a longer line fracture  $\gamma = Q_1Q_2$  with two vertices  $Q_1 = (0.1, 0.5)$ ,  $Q_2 = (0.9, 0.5)$ . See Fig. 8 for the initial mesh and the graded mesh with  $\kappa = 0.2$  after four refinements. The convergence rates associated with different values of  $\kappa = \kappa_{Q_1} = \kappa_{Q_2}$  are reported in the second column of Table 2. Similar to the numerical tests in Example 5.1, these results show that the convergence rate is suboptimal with  $e = 0.93$  on the quasi-uniform mesh ( $\kappa = 0.5$ ), but becomes optimal ( $e = 1$ ) on graded meshes for  $\kappa < 0.5$ .

**Test 2.** We consider a line fracture  $\gamma = Q_1Q_2$  with the two vertices  $Q_1 = (0.2, 0.2)$ ,  $Q_2 = (0.8, 0.8)$ . Here we solve the problem (1.1) on graded meshes with the initial triangulation given in Fig. 9. The convergence rate is reported in the third column of Table 2. We observe that convergence rate is suboptimal with  $e = 0.94$  on quasi-uniform mesh ( $\kappa = 0.5$ ), but it is optimal ( $e = 1$ ) on graded meshes for  $\kappa < 0.5$ . The results in Table 2, both from Test 1 and Test 2, are well predicted by the theory as discussed above.

**Test 3.** In this test, we consider two line fractures with  $\gamma_1 = Q_1Q_2$ ,  $\gamma_2 = Q_3Q_4$  in Eq. (1.1). Here the vertices are  $Q_1 = (0.3, 0.1)$ ,  $Q_2 = (0.3, 0.9)$ ,  $Q_3 = (0.6, 0.1)$  and  $Q_4 = (0.9, 0.9)$ . The initial mesh is given in Fig. 10. Although two

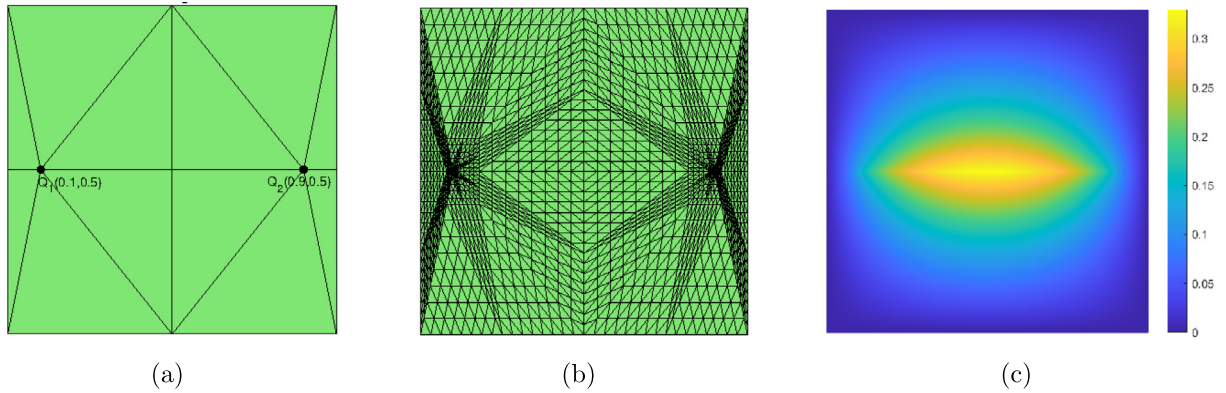


**Fig. 8.** Graded meshes with line fracture  $\gamma = Q_1Q_2$ ,  $Q_1 = (0.1, 0.5)$ ,  $Q_2 = (0.9, 0.5)$ . (a) the initial mesh; (b) the mesh after four refinements,  $\kappa = \kappa_{Q_1} = \kappa_{Q_2} = 0.2$ ; (c) the numerical solution.

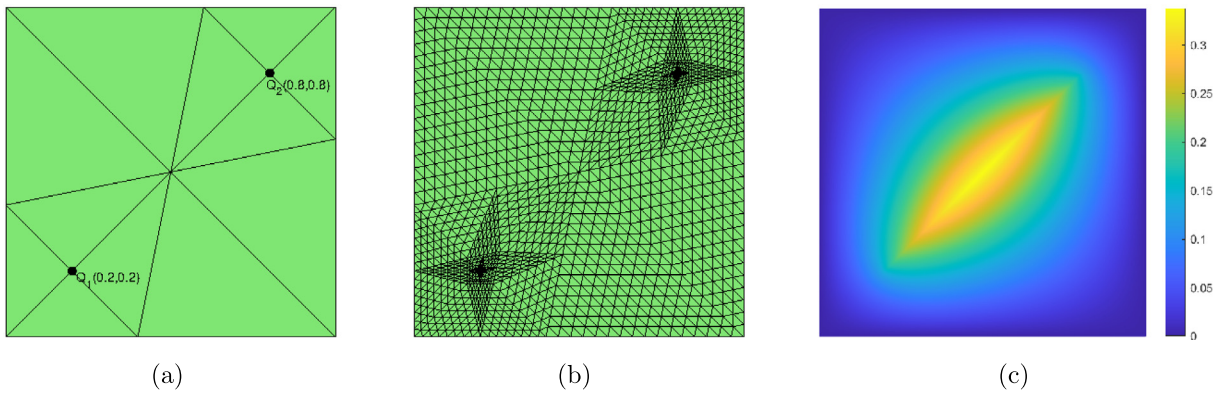


**Fig. 9.** Graded meshes with line fracture  $\gamma = Q_1Q_2$ ,  $Q_1 = (0.2, 0.2)$ ,  $Q_2 = (0.8, 0.8)$ . (a) the initial mesh; (b) the mesh after four refinements,  $\kappa = \kappa_{Q_1} = \kappa_{Q_2} = 0.2$ ; (c) the numerical solution.

**Table 2**  
Convergence history in Tests 1 & 2 of Example 5.2 on graded meshes.

$\kappa \setminus j$	$j = 4$	$j = 5$	$j = 6$	$j = 7$	$j = 4$	$j = 5$	$j = 6$	$j = 7$
$\kappa = 0.1$	0.97	0.98	0.99	1.00	0.97	0.99	0.99	1.00
$\kappa = 0.2$	0.98	0.99	1.00	1.00	0.97	0.99	1.00	1.00
$\kappa = 0.3$	0.99	1.00	1.00	1.00	1.00	1.00	1.00	1.00
$\kappa = 0.4$	0.95	0.97	0.98	0.99	0.96	0.98	0.99	0.99
$\kappa = 0.5$	0.91	0.92	0.93	0.93	0.93	0.93	0.94	0.94

**Table 3**  
Convergence history in Test 3 of Example 5.2 on graded meshes.

$\kappa \setminus j$	$j = 4$	$j = 5$	$j = 6$	$j = 7$
$\kappa = 0.1$	0.98	0.99	1.00	1.00
$\kappa = 0.2$	1.00	1.00	1.00	1.00
$\kappa = 0.3$	0.99	1.00	1.00	1.00
$\kappa = 0.4$	0.96	1.00	1.00	1.00
$\kappa = 0.5$	0.92	0.93	0.93	0.94

line fractures are imposed, we also observe similar convergence rates (see Table 3): the suboptimal convergence rate with  $e = 0.94$  on quasi-uniform meshes ( $\kappa = 0.5$ ), and optimal ( $e = 1$ ) on graded meshes as  $\kappa := \kappa_{Q_1} = \kappa_{Q_2} = \kappa_{Q_3} = \kappa_{Q_4} < 0.5$ .

In Test 1 and Test 2, we have implemented linear finite element methods proposed in Algorithm 4.1. These numerical test results are in strong support of the estimate in Theorem 4.8. We chose the square domain to avoid the possible corner singularity due to the non-smoothness of the domain, so that we can concentrate on the singular solution in the



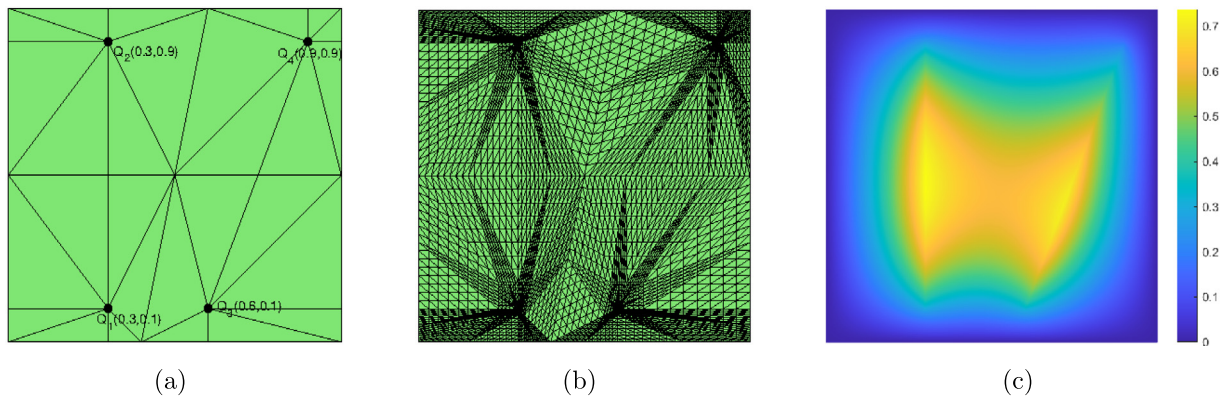


**Fig. 10.** Graded meshes with two line fractures  $\gamma_1 = Q_1Q_2$  and  $\gamma_2 = Q_3Q_4$ . (a) the initial mesh; (b) the mesh after four refinements,  $\kappa = \kappa_{Q_1} = \kappa_{Q_2} = \kappa_{Q_3} = \kappa_{Q_4} = 0.2$ ; (c) the numerical solution.

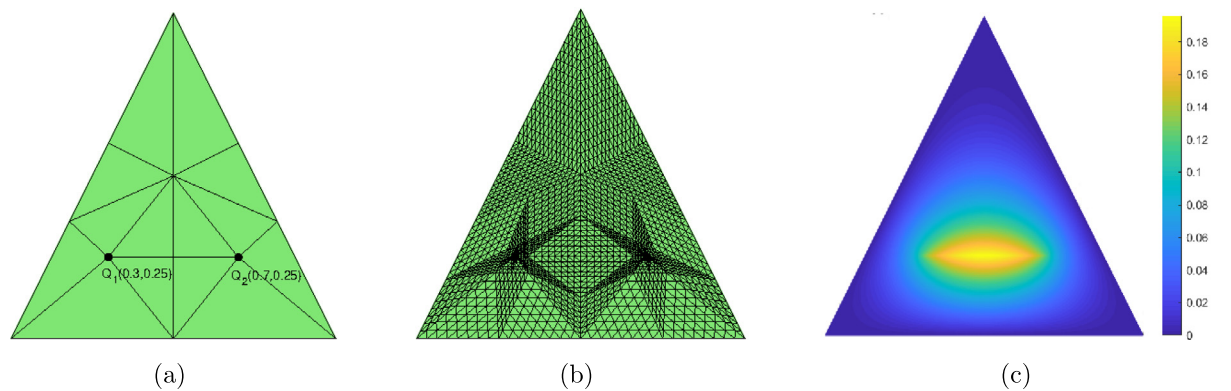


**Fig. 11.** Quadratic finite element methods on graded meshes with the line fracture  $\gamma = Q_1Q_2$ ,  $Q_1 = (0.3, 0.25)$ ,  $Q_2 = (0.7, 0.25)$ . (a) the initial mesh; (b) the mesh after four refinements,  $\kappa = \kappa_{Q_1} = \kappa_{Q_2} = 0.2$ ; (c) the numerical solution.

**Table 4**  
Convergence history of the  $P_2$  elements in Example 5.3 on graded meshes.

$\kappa \setminus j$	$j = 4$	$j = 5$	$j = 6$	$j = 7$
$\kappa = 0.1$	1.74	1.86	1.94	1.97
$\kappa = 0.2$	1.81	1.88	1.93	1.97
$\kappa = 0.3$	1.65	1.68	1.70	1.71
$\kappa = 0.4$	1.32	1.32	1.32	1.32
$\kappa = 0.5$	1.00	1.00	1.00	1.00

neighborhood of the line fracture. For general polygonal domains, the corner singularities should be taken into account. A proper refinement algorithm near these corners are also given in Remark 4.2 and Theorem 4.8.

**Example 5.3 ( $P_2$  Finite Element Methods).** In this example, we consider the finite element method based on  $P_2$  polynomials for Eq. (1.1). To minimize the effect of potential corner singularities, we solve the equation in the triangle domain  $\Omega = \triangle ABC$  with  $A = (0, 0)$ ,  $B = (1, 0)$  and  $C = (0.5, 1)$  and the line fracture  $\gamma = Q_1Q_2$  with the two vertices  $Q_1 = (0.3, 0.25)$ ,  $Q_2 = (0.7, 0.25)$ . Since all the interior angles of  $\Omega$  are less than  $\frac{\pi}{2}$ , the solution is in  $H^3$  except for the region that contains  $\gamma$ . See Fig. 11 for the initial triangulation that conforms to the fracture. Based on Theorem 4.8, to achieve the optimal convergence rate in the numerical approximation, it is sufficient to use quasi-uniform meshes near the vertices of the domain and use graded meshes with the grading parameter  $\kappa := \kappa_{Q_1} = \kappa_{Q_2} = 2^{-\frac{2}{a}} < 0.25$  due to the fact  $0 < a < 1$ .

The convergence rate (5.1) of the numerical solution in this example is reported in Table 4. We observe that the convergence rate is suboptimal on graded meshes with  $\kappa > 0.25$ . In particular,  $e = 1$  on quasi-uniform meshes ( $\kappa = 0.5$ ) and  $1 < e < 2$  on graded meshes with  $\kappa = 0.3, 0.4$ . It is clear that the optimal convergence rate  $e = 2$  is obtained on graded meshes when  $\kappa < 0.25$ . These numerical results are clearly consistent with the theory developed in this paper.

## Acknowledgments

This research was supported in part by the National Science Foundation, United States of America Grant DMS-1819041 and by the Wayne State University, United States of America Faculty Competition for Postdoctoral Fellows Award.

## References

- [1] C. D'Angelo, Finite element approximation of elliptic problems with Dirac measure terms in weighted spaces: applications to one- and three-dimensional coupled problems, *SIAM J. Numer. Anal.* 50 (1) (2012) 194–215.
- [2] W. Gong, G. Wang, N. Yan, Approximations of elliptic optimal control problems with controls acting on a lower dimensional manifold, *SIAM J. Control Optim.* 52 (3) (2014) 2008–2035.
- [3] I. Babuška, Error-bounds for finite element method, *Numer. Math.* 16 (1971) 322–333.
- [4] R. Scott, Finite element convergence for singular data, *Numer. Math.* 21 (1973) 317–327.
- [5] R. Scott, Optimal  $L^\infty$  estimates for the finite element method on irregular meshes, *Math. Comp.* 30 (1976) 681–697.
- [6] E. Casas,  $L^2$  Estimates for the finite element method for the Dirichlet problem with singular data, *Numer. Math.* 47 (1985) 627–632.
- [7] T. Köppl, B. Wohlmuth, Optimal a priori error estimates for an elliptic problem with Dirac right-hand side, *SIAM J. Numer. Anal.* 52 (4) (2014) 1753–1769.
- [8] K. Eriksson, Improved accuracy by adapted mesh-refinements in the finite element, *Math. Comp.* 44 (170) (1985) 321–343.
- [9] T. Apel, O. Benedix, D. Sirch, B. Vexler, A priori mesh grading for an elliptic problem with Dirac right-hand side, *SIAM J. Numer. Anal.* 49 (3) (2011) 992–1005.
- [10] L. Heltai, N. Rotundo, Error estimates in weighted Sobolev norms for finite element immersed interface methods, *Comput. Math. Appl.* 78 (11) (2019) 3586–3604.
- [11] L. Heltai, W. Lei, A priori error estimates of regularized elliptic problems, *Numer. Math.* 146 (2020) 571–596.
- [12] C. D'Angelo, A. Quarteroni, On the coupling of 1D and 3D diffusion-reaction equations. Application to tissue perfusion problems, *Math. Models Methods Appl. Sci.* 18 (8) (2008) 1481–1504.
- [13] S. Ariche, C. De Coster, S. Nicaise, Regularity of solutions of elliptic or parabolic problems with Dirac measures as data, *SeMA J.* 73 (2016) 379–426.
- [14] J. Lions, E. Magenes, *Non-Homogeneous Boundary Value Problems and Applications*, Vol. 1, Springer-Verlag, 1972.
- [15] S. Kesavan, *Topics in Functional Analysis and Applications*, first ed., in: *Topics in Functional Analysis and Applications*, New Age International Publishers, Wiley, New York, 1989.
- [16] S. Alinhac, P. Gérard, S.S. Wilson, *Pseudo-Differential Operators and the Nash-Moser Theorem*, in: *Stud. Math.*, vol. 82, AMS, Providence, RI, 2007.
- [17] Philippe G. Ciarlet, *The Finite Element Method for Elliptic Problems*, Université Pierre et Marie Curie, Paris, France, 1974.
- [18] T. Apel, *Anisotropic finite elements: local estimates and applications*, in: *Advances in Numerical Mathematics*, B. G. Teubner, Stuttgart, 1999.
- [19] M. Dauge, *Elliptic Boundary Value Problems on Corner Domains*, in: *Lecture Notes in Mathematics*, vol. 1341, Springer-Verlag, Berlin, 1988.
- [20] P. Grisvard, *Elliptic Problems in Nonsmooth Domains*, in: *Monographs and Studies in Mathematics*, vol. 24, Pitman (Advanced Publishing Program), Boston, MA, 1985.
- [21] V. Kondrat'ev, Boundary value problems for elliptic equations in domains with conical or angular points, *Trudy Moskov. Mat. Obšč.* 16 (1967) 209–292.
- [22] H. Li, A. Mazzucato, V. Nistor, Analysis of the finite element method for transmission/mixed boundary value problems on general polygonal domains, *Electron. Trans. Numer. Anal.* 37 (2010) 41–69.
- [23] S. Nicaise, *Polygonal Interface Problems*, Lang, Peter Publishing, Incorporated, 1993.
- [24] C. Băcuță, V. Nistor, L.T. Zikatanov, Improving the rate of convergence of 'high order finite elements' on polygons and domains with cusps, *Numer. Math.* 100 (2) (2005) 165–184.
- [25] H. Li, V. Nistor, Analysis of a modified Schrödinger operator in 2D: regularity, index, and FEM, *J. Comput. Appl. Math.* 224 (2009) 320–338.